Artificial Nacre

DOI: 10.1002/anie.201210166

Ultratough Artificial Nacre Based on Conjugated Cross-linked Graphene Oxide**

Qunfeng Cheng, Mengxi Wu, Mingzhu Li,* Lei Jiang, and Zhiyong Tang**

Natural nacre, which consists of almost 95 vol% inorganic content (calcium carbonate) and 5 vol% elastic biopolymers, possesses a unique combination of remarkable strength and toughness,[1] which is attributed to its hierarchical nano-/microscale structure and precise inorganic–organic interface.[2] Inspired by the intrinsic relationship between the structures and the mechanical properties lying in the natural nacre, different types of nacre-like layered nanocomposites have been fabricated with two-dimensional (2D) inorganic additives, including glass flake,[3] alumina flake,[4] graphene oxide,[5] layered double hydroxides,[6] nanoclay,[7] and flattened double-walled carbon nanotubes.[8] Although great progress has been achieved in tensile mechanical properties,[7b,c,8,9] in only very rare cases are artificial layered composites with excellent toughness are obtained.[6,10] One of the most important causes is the relatively low interfacial strength between interlayers of artificial nacre. Recently, 2D graphene has attracted much research interest owing to its outstanding electrical, thermal, and mechanical properties,[11] and many graphene-based devices have been fabricated,[12] such as bulk composites,[13] one-dimensional fibers,[14] supercapacitors.[15] As the water-soluble derivative of graphene, graphene oxide (GO), with many functional groups on the surface, is one of the best candidates for fabricating artificial nacre, because functional surface groups allow for chemical cross-linking to improve the interfacial strength of the adjacent GO layers. Until now, several methods have been developed to functionalize individual GO sheets and enhance the resultant mechanical properties, including divalent ion (Mg^{2+}, Ca^{2+}) modification,[16] polyallylamine[17] or alkylamine[18] functionalization, borate cross-linking,[19] glutaraldehyde (GA) treatment,[20] π–π interactions,[21] and hydrogen bonding.[22] Although the obtained strength and stiffness are significantly enhanced, the modified materials are always accompanied by a reduced ductility or toughness.[19] In a brief, it still remains a great challenge to obtain the ultratough artificial nacre based on the 2D GO sheets.

Herein, inspired by the relationship of excellent toughness and hierarchical nano-/microscale structure of the natural nacre, we have developed a novel strategy for fabricating the ultratough artificial nacre based on 2D GO sheets by conjugated cross-linking. Highly π-conjugated long-chain polymers made of 10,12-pentacosadiyn-1-ol (PCDO) monomers[23] are cross-linked with the GO sheets, resulting in a huge displacement upon loading and adsorption of much more fracture energy. The toughness is two times higher than that of the natural nacre. Furthermore, the π-conjugated polymers could add additional benefit to the high electrical conductivity of the chemically reduced GO (rGO). It is expected that this novel type of the ultratough and conductive artificial nacre has great potential in aerospace,[24] flexible supercapacitor electrodes,[15] artificial muscles,[25] and tissue engineering.[26]

The typical hierarchical nano-/microscale structure of natural nacre is shown in Figure 1 a–c. $CaCO_3$ platelets with a thickness of 200–500 nm are assembled into the layered nanocomposites. The nanoasperities on the surface of the $CaCO_3$ platelets play a key role in the process of dissipating crack energy when loading, through typical toughening mechanisms such as crack deflecting,[27] interlocking,[28] and mineral bridging.[29] Inspired by the relationship of outstanding toughness with the hierarchical nano-/microscale structure of natural nacre, we assembled 2D GO sheets and π-conjugated polymer PCDO into the ultratough artificial nacre. The inorganic GO sheets act as the bricks, while the PCDO polymers act as the mortar in the artificial nacre. Thermogravimetric analysis reveals that the weight loading of the PCDO in the composites is about 6.5 wt%, which is comparable to natural nacre (Supporting Information, Figure S1). In contrast to natural nacre, PCDO is not only the organic phase of the artificial nacre, but also the cross-linker of adjacent GO sheets. The long chain of the PCDO causes

[*] Prof. Q. F. Cheng, Dr. M. X. Wu, Prof. L. Jiang
Key Laboratory of Bio-inspired Smart Interfacial Science and Technology of Ministry of Education
School of Chemistry and Environment
BeiHang University, Beijing 100191 (P. R. China)
E-mail: cheng@buaa.edu.cn
Prof. M. Z. Li
Laboratory of New Materials, Institute of Chemistry
Chinese Academy of Science, Beijing 100190 (P. R. China)
E-mail: mingzhu@iccas.ac.cn
Prof. Z. Y. Tang
National Center for Nanoscience and Technology
Beijing 100190 (P. R. China)
E-mail: zytang@nanoctr.cn

[**] This work was supported by the National Research Fund for Fundamental Key Projects (2010CB934700, 2009CB930401), the National Natural Science Foundation of China (21273017, 51103004, 21003132, 91127038, 20920102036, 209774113, 91027011), the Research Fund for the Doctoral Program of Higher Education (20101102120044), the Fundamental Research Funds for the Central Universities (YWF-12-LXGY-017), the National Natural Science Foundation for Distinguished Youth Scholars of China (21025310), Program for New Century Excellent Talents in University (NCET-12-0034), Beijing Nova Program (Z121103002512020), Beijing Science and Technology Program (Z121100001312004), and the Key Research Program of the Chinese Academy of Sciences (KJZD-EW-M01).

Supporting information for this article is available on the WWW under http://dx.doi.org/10.1002/anie.201210166.

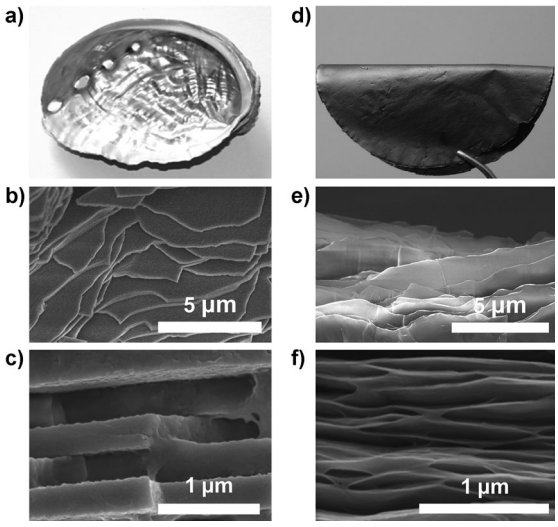

Figure 1. Comparison of natural nacre with artificial nacre based on graphene oxide (GO): a) Image of the shellof red abalone. b),c) SEM images of the cross-section of natural red abalone shell, showing unique arrangement of the $CaCO_3$ platelets in the multilayered composite. d) Photo of artificial nacre. e),f) SEM images of the cross-section of artificial nacre based on GO, showing the multilayer structure of the assembled GO sheets cross-linked with the PCDO.

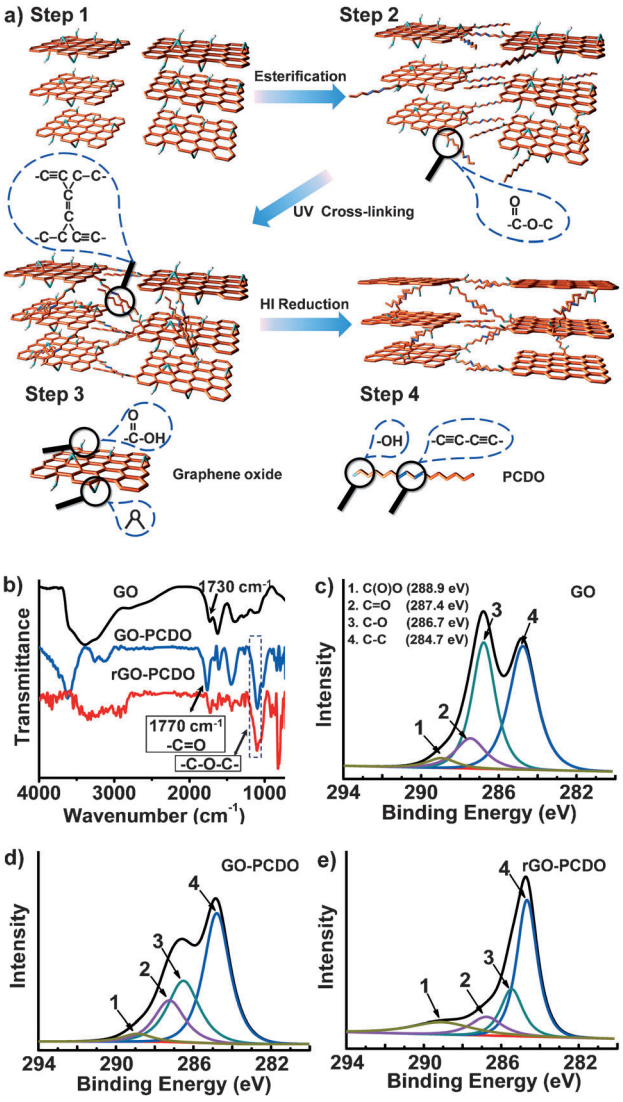

Figure 2. a) The fabrication procedure for ultratough and conductive artificial nacre based on GO and PCDO. b) FTIR spectra of pure GO films, GO-PCDO composites, and rGO-PCDO composites. Peaks at 1100–1250 cm^{-1} and 1770 cm^{-1} indicate successful grafting of PCDO on the surface of GO-PCDO and rGO-PCDO. c–e) XPS spectra of pure GO films, GO-PCDO composites, and rGO-PCDO composites. The decrease in the peak intensity of C=O and C–O after HI reduction shows the removal of the unreacted functional groups.

huge slippage when loading, and the excellent toughness, which is two times higher than that of the natural nacre, is easily achieved with the artificial nacre (Figure 1 d). Figure 1 e demonstrates the fracture morphology of the artificial nacre, and pulling out of the rGO sheets can be clearly discerned. The fracture path is obviously different with other reported rGO reinforced polymer composites, but identical to the natural nacre (Figure 1 b). A cross-sectional image of the artificial nacre shows a typical layered structure (Figure 1 f), which is also comparable to natural nacre (Figure 1 c).

To assemble the GO sheets, the sheets were first dispersed into deionized water. The thickness of individual GO sheets was measured to be about 1.0 nm by atomic force microscopy imaging (Supporting Information, Figure S2). Subsequently, the GO dispersion was infiltrated with the use of vacuum and assembled into the layered GO films (Figure 2 a, step 1). The PCDO was then introduced into the pre-formed GO films by soaking the GO films in a pre-mixed tetrahydrofuran/PCDO solution. After several hours, the esterification reaction between the alcohol at one end of the PCDO molecules and carboxylic acids on the surface of the GO sheets was complete, and the PCDO monomers were grafted on the surface of the GO sheets (Figure 2 a, step 2). To improve the interfacial strength and conductivity of the resultant composites, the PCDO molecules were cross-linked by 1,4-addition polymerization of their diacetylenic units under UV irradiation (Figure 2 a, step 3).[23] X-ray diffraction (XRD) results showed that the interlayer distance of the GO-PCDO composites was increased from 7.596 Å ($2\theta = 11.64°$) to 7.978 Å ($2\theta = 11.08°$) in respect to the pure GO films, suggesting that the PCDO was successfully embedded into the GO films (Supporting Information, Figure S3). Finally, the GO-PCDO composites were reduced by hydroiodic acid (HI) solution, not only aiming at removal of the unreacted chemical groups on the GO sheets but also improvement of the conductivity of the synthesized composites (Figure 2 a, step 4). The distance of the reduced GO-PCDO (rGO-PCDO) was decreased to 3.666 Å ($2\theta = 24.26°$), higher than 3.648 Å ($2\theta = 24.38°$) of the pure rGO films, indicating that after reduction, the PCDO polymers were still immobilized among the rGO sheets. The successful introduction of the PCDO into the rGO films is also proved by spectroscopic characterization. As for the pure GO films, the peak at 1730 cm^{-1} in FTIR spectrum is assigned to the stretching vibration of the carboxylic acid (Figure 2 b, black curve). After esterification, the carboxylic acid peak at 1730 cm^{-1} is

weakened, accompanying with appearance of strong peaks at 1100–1250 cm^{-1} corresponding to the stretching vibration of the −C−O−C moiety in ester groups and at 1770 cm^{-1} corresponding to the stretching vibration of the C=O moiety in ester groups (blue curve). It is evident that all these characteristic peaks are kept intact after HI reduction (red curve), confirming the strong esterification between the PCDO and the GO sheets. Though the PCDO polymers are stably attached on the GO surfaces, HI reduction could give rise to considerable elimination of the unreacted groups on the surface of the rGO sheets, which is shown by X-ray photoelectron spectroscopy (XPS; Figure 2c,d,e). The broad C_{1s} peak of both the pure GO and the GO-PCDO can be fitted into four peaks with the binding energy at 284.7, 286.7, 287.4, and 288.9 eV, corresponding to the C−C, C−O, C=O, and C(O)O groups, respectively. The peak intensity of C=O and C−O of the GO-PCDO composites is significantly decreased after chemical reduction by HI. Accordingly, the ratio of O_{1s} to C_{1s} is decreased significantly after HI reduction.

The electronic structure change in the GO sheets after chemical functionalization with the PCDO was explored by Raman spectra (Supporting Information, Figure S4). After grafting of the PCDO, the intensity ratio of the D band (ca. 1300 cm^{-1}) to G band (ca. 1590 cm^{-1}), the D/G ratio, increased from 0.923 for the pure GO films to 0.954 for the GO-PCDO composites. Analogously, after HI reduction, the D/G ratio is increased from 1.151 of the rGO films to 1.178 of the rGO-PCDO composites. The details characterization results from XRD, Raman, and XPS spectroscopy is listed in the Supporting Information, Table S1. The above results highlight that the cross-linking bonds with the PCDO would simultaneously provide the strong interface strength and the electron-transfer path between the GO sheets.

Typical stress–strain curves of the prepared samples are shown in Figure 3a. The tensile strength and toughness of the pure GO films are 95.4 ± 3.9 MPa and 0.37 ± 0.06 MJ m^{-3}, respectively, which are similar to the previously reported values.[30] Owing to the weak hydrogen bonds between the adjacent GO sheets, the strength and toughness of the pure GO films are lower than those of the natural nacre (tensile strength of 80–135 MPa and toughness of 1.8 MJ m^{-3}).[28] When the PCDO molecules are grafted on the GO sheets and cross-linked together, the tensile strength is increased to 106.6 ± 17.1 MPa, which is comparable to that of natural nacre, while the toughness is dramatically raised to 2.52 ± 0.59 MJ m^{-3}, which is about 40% higher than that of natural nacre. As the graphene sheets exhibit much higher mechanical and electrical properties in respect to the GO sheets,[31] many methods have been developed to reduce the GO sheets into the rGO sheets by removing the oxygen-containing groups with recovery of the conjugated structure.[32] In this study, HI is used to reduce the GO sheets.[33] After reduction, the tensile strength and toughness of the pure rGO films are increased to 111.2 ± 14.5 MPa and 1.49 ± 0.03 MJ m^{-3}, respectively. As for the artificial nacre of the rGO-PCDO composites, the average tensile strength is increased to 129.6 ± 18.5 MPa, and the maximum value can reach 156.8 MPa, which is higher than that of natural nacre. More remarkably, the toughness of the rGO-PCDO composites is up to 3.91 ± 0.03 MJ m^{-3}, which is two times higher than that of natural nacre. The excellent mechanical properties of the rGO-PCDO composites are attributed to the layered hierarchical

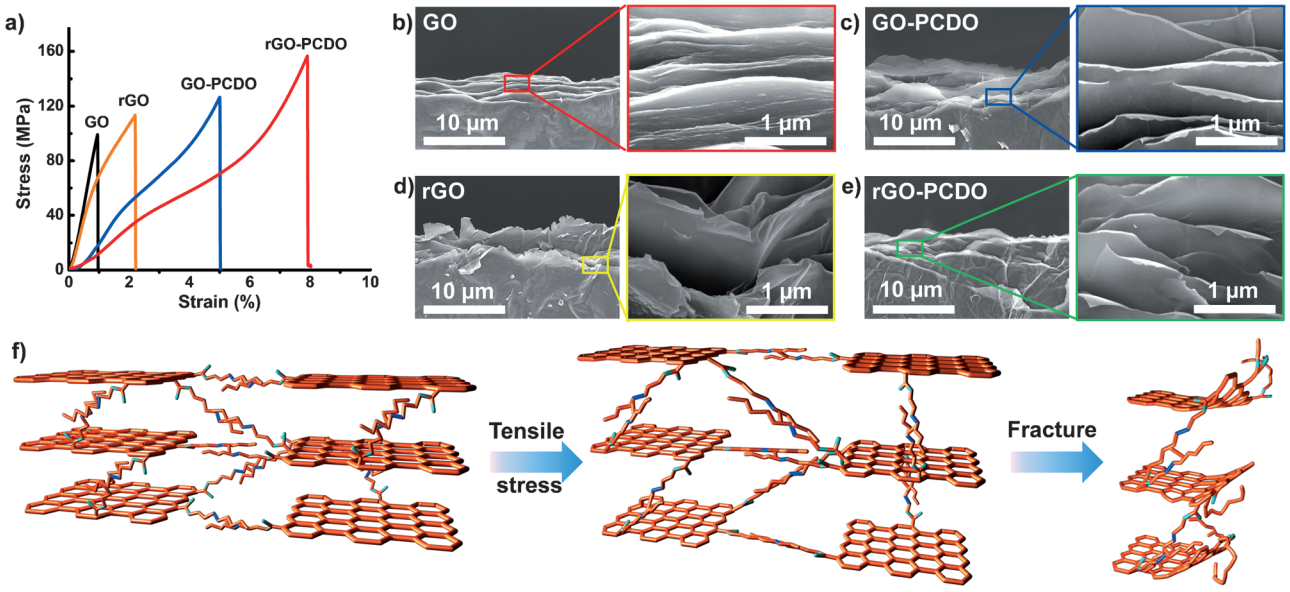

Figure 3. Mechanical properties of GO film and GO-PCDO composites before and after reduction. a) Stress–strain curves of GO films, rGO films, GO-PCDO composites, and rGO-PCDO composites. b)–e) SEM images of pure GO films, pure rGO films, GO-PCDO composites, and rGO-PCDO composites, showing the difference in the fracture morphologies. The GO films show a typical brittle fracture morphology without any pulling out of the GO sheets owing to the weak interfacial bonding between the adjacent GO sheets. As a comparison, the GO and rGO sheets of the artificial nacre are pulled out and curved owing to the breaking of the chemical bonds between GO and rGO with PCDO. f) The fracture path of the rGO-PCDO composites upon loading. The curled long chain of PCDO is gradually stretched and broken with loading, simultaneously resulting in curving of the edges of the rGO sheets.

nano-/microscale structure and the unique chemical cross-linking with the PCDO polymers.

Detailed structural analysis was performed to understand the intrinsic factors to improve the mechanic strength. The pure GO films show a typical brittle fracture morphology without any pulling out of the GO sheets (Figure 3b), which is similar to the previous report.[30] After cross-linking with the PCDO, many GO sheets are observed to be pulled out owing to the strong interactions between the adjacent GO sheets (Figure 3c). In particular, it can be seen that the edges of the GO sheets are curved rather than flattened, indicating that breakage of the covalent bonds between the PCDO and the GO brings about obvious deformation of the GO sheets and would cost more energy (magnified image in Figure 3c). After HI reduction, the rGO-PCDO composites (Figure 3e) have identical fracture morphology to that of the GO-PCDO composites, and the edges of the rGO sheets show even more strongly curved. There are both similarity and difference in the fracture morphologies between the GO-PCDO composites and the natural nacre. In both samples, 2D platelets are irregularly pulled out. However, the GO sheets have the curved morphology owing to their flexibility, and the $CaCO_3$ platelets remain flattened owing to their brittleness. The novel fracture morphology of the GO sheets demonstrates that although the artificial nacre based on the GO sheets exhibits high strength and toughness, the full potential of the mechanical properties of GO sheets has not yet to be exploited considering their superhigh mechanical properties. Further improvements in the interfacial bonding and load transfer could be expected to offer much higher mechanical performance.

The whole fracture process of the rGO-PCDO composites under tensile stress is shown in Figure 3f. In the layered structure of the rGO-PCDO composites, the organic PCDO molecules are grafted on the 2D inorganic rGO sheets through the covalent ester bonds, while the PCDO molecules form intercross-linked networks through conjugation of ene–yne backbones and adopt a randomly coiled conformation. When loading, the rGO sheets extensively slide against each other. The weak hydrogen bonds between the rGO sheets are firstly ruptured, followed by stretching of the coiled PCDO long chains along the sliding direction, resulting in dissipation of a large amount of energy. When loading is further increased, the chemical bonds between the PCDO and the rGO sheets, as well as the ene–yne backbones in the conjugated PCDO, are broken, simultaneously resulting in curving of the rGO sheets.

The mechanical performance of the GO-PCDO and rGO-PCDO composites with those of the natural materials, including nacre, bone, and detin, as also different GO- or rGO-based composites, are compared in Figure 4. Impressively, the artificial nacre shows much better mechanical properties. The maximum tensile strength of the rGO-PCDO composites can reach 156.8 MPa, which is higher than that of natural nacre (tensile strength of 80–135 MPa),[28] bone (tensile strength of 150 MPa),[34] and dentin (tensile strength of 105.5 ± 16.4 MPa).[35] The toughness of the rGO-PCDO composites is up to 3.91 ± 0.03 MJ m^{-3}, which is two times higher than that of the natural nacre (1.8 MJ m^{-3}),[28] three times higher than that of bone (1.2 MJ m^{-3}),[34] and 1.9 times higher than that of dentin (2.0 MJ m^{-3}).[35] On the other hand, our strategy to fabricate the GO-based composites is also superior to other approaches of different cross-linking agents, such as divalent ion (Mg^{2+}, Ca^{2+}) modification,[16] borate cross-linking,[19] glutaraldehyde (GA) treatment,[20] hydrogen bonding,[22] and nacre-like composites based on GO and poly(acrylic acid) (PAA),[17] poly(allylamine hydrochloride) (PAH),[36] poly(vinyl alcohol) (PVA),[5a,37] and poly(methyl methacrylate) (PMMA).[37] A comparison of mechanical properties of our artificial nacre with the natural nacre and other GO-based composites is listed in the Supporting Information, Table S2. The currently used cross-linking strategies are mostly responsible for improving the tensile strength instead of the toughness of the GO-based materials. In contrast, thanks to the coiled feature of the long chain of the PCDO, the rGO-PCDO composites have much higher strength and toughness. For example, the appropriate hydrogen bonding (H-bond) interactions between the adjacent GO sheets by incorporating water molecules[22] can only achieve less than 10% improvement in stiffness and 1% improvement in tensile strength, as the H-bond interaction energy is relatively weak.[38] The effective borate cross-linking inspired by *Triticum aestivum* plants can achieve improvements of 255% in stiffness and 25% in strength with addition of 0.94 wt% boron.[19] However, the failure strain is dramatically decreased to only 0.15% and the corresponding toughness is only 0.14 MJ m^{-3}.

The conjugated areas in the GO sheets are usually destroyed in the process of exfoliation from graphite by chemical treatment, so that the GO sheets are typically insulating.[39] Reduction of GO not only can remove most of the oxygen-containing groups and other atomic-scale lattice defects, but also recover the conjugated network of the graphitic lattice.[32] After reduction by HI, the electrical conductivity of the rGO films is increased to 49.30 S cm^{-1}, which is comparable to the reported pure rGO films (50 S cm^{-1}).[5d] Interestingly enough, the rGO-PCDO composites shows a much higher electrical conductivity of 232.29 S cm^{-1}, which is four times higher than that of the

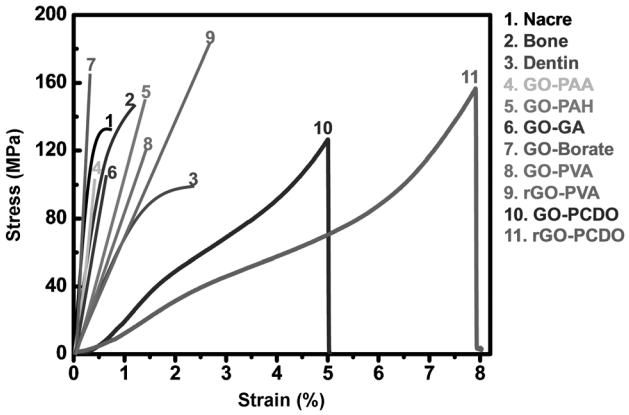

Figure 4. Comparison of stress–strain curves of our artificial nacre of GO-PCDO and rGO-PCDO composites with the natural nacre, bone, dentin, and other GO or rGO films with different cross-linking strategies.

rGO-PVA composites (52.65 $S\,cm^{-1}$)[5a] and three times higher than that of rGO film reduced by hydrazine (72 $S\,cm^{-1}$).[40] Both the thoroughly rGO sheets and the π-conjugated backbones of the cross-linked PCDO contributes to such an exceptionally high electrical conductivity of the rGO-PCDO composites. The ultratough and conductive artificial nacre is quite unique, and has many potential applications in electrical devices and could be used as the supercapacitor electrodes.

In conclusion, inspired by natural nacre, we successfully fabricated GO-based composites. In comparison with previous preparation methods, this novel cross-linking strategy demonstrates the following crucial advantages: 1) It dramatically decreases the content of organic polymers in the resultant composites, which is comparable to the natural nacre; 2) it produces the distinct inorganic–organic layered hierarchical nano-/microstructures; 3) it realizes integration of the high tensile strength and excellent toughness; and 4) it creates highly conductive composites based on GO and conjugated molecules. This study opens the door toward biomimetic production of the GO- or rGO-based composites of superior toughness and high conductivity, which will have great promising applications in many fields, such as aerospace, flexible supercapacitor electrodes, artificial muscles, and tissue engineering.

Experimental Section

GO was purchased from XianFeng NANO Co., Ltd. 10,12-pentacosadiyn-1-ol (PCDO) was purchased from Tokyo Chemical Industry Co., Ltd., and 57 wt% HI acid was purchased from Sigma–Aldrich.

Fabrication of GO films: GO was dispersed in deionized water. Exfoliation was performed by sonicating an aqueous suspension of GO (100 mL, 20 $mg\,mL^{-1}$) for 1 h. Un-exfoliated aggregates were removed from the solution by centrifugation, and the supernatant solution was collected. The GO films were assembled by vacuum-assisted filtration, followed by air drying and peeling from the filter.

Preparation of rGO-PCDO composites: The GO films were immersed in a PCDO solution. Subsequently, the PCDO-grafted GO films were treated under UV irradiation at a wavelength of 365 nm. The final GO-PCDO composites were rinsed, and the resultant GO-PCDO composites were reduced by HI solution. Finally, the rGO-PCDO composites were obtained after washing and drying.

Mechanical properties were evaluated using a Shimadzu AGS-X Tester at a loading rate of 1 $mm\,min^{-1}$ with a gauge length of 5 mm. All of the samples were cut into strips with the length of 20 mm and the width of 3 mm. Scanning electron microscopy (SEM) images were obtained by the HITACHI S-4800. The atomic force microscopy were characterized by a Leica TCS SP5. The thermogravimetric analysis was performed on TG/DTA6300, NSK under N_2 with a temperature rising rate of 5 °C min^{-1}. All of the X-ray photoelectron spectroscopy (XPS) measurements were taken in an ESCALab220i-XL (Thermo Scientific) using a monochromatic Al-Kα X-ray source. Raman spectroscopy measurements were taken using a LabRAM HR800 (Horiba Jobin Yvon) with the excitation energy of 2.54 eV (488 nm). X-ray diffraction (XRD) experiments were carried out with a D/max-2500 (Rigaku) instrument using Cu-Kα radiation. FTIR spectra were collected using a Thermo Nicolet nexus-470 FTIR instrument.

Received: December 20, 2012
Published online: February 11, 2013

Keywords: artificial nacre · cross-linking · graphene oxide · ultratough materials

[1] a) Z. Huang, H. Li, Z. Pan, Q. Wei, Y. J. Chao, X. Li, *Sci. Rep.* **2011**, *1*, 148; b) Z. Huang, X. Li, *Phys. Rev. Lett.* **2012**, *109*, 025501; c) X. Li, Z. Huang, *Phys. Rev. Lett.* **2009**, *102*, 075502; d) X. Li, Z.-H. Xu, R. Wang, *Nano Lett.* **2006**, *6*, 2301.

[2] a) H.-B. Yao, H.-Y. Fang, X.-H. Wang, S.-H. Yu, *Chem. Soc. Rev.* **2011**, *40*, 3764; b) J. Wang, Q. Cheng, Z. Tang, *Chem. Soc. Rev.* **2012**, *41*, 1111; c) H. D. Espinosa, J. E. Rim, F. Barthelat, M. J. Buehler, *Prog. Mater. Sci.* **2009**, *54*, 1059.

[3] H. Kakisawa, T. Sumitomo, R. Inoue, Y. Kagawa, *Compos. Sci. Technol.* **2010**, *70*, 161.

[4] a) O. Oner Ekiz, A. F. Dericioglu, H. Kakisawa, *Mater. Sci. Eng. C* **2009**, *29*, 2050; b) L. J. Bonderer, K. Feldman, L. J. Gauckler, *Compos. Sci. Technol.* **2010**, *70*, 1958.

[5] a) Y.-Q. Li, T. Yu, T.-Y. Yang, L.-X. Zheng, K. Liao, *Adv. Mater.* **2012**, *24*, 3426; b) J. Zhu, C. M. Andres, J. Xu, A. Ramamoorthy, T. Tsotsis, N. A. Kotov, *ACS Nano* **2012**, *6*, 8357; c) Y. Xu, W. Hong, H. Bai, C. Li, G. Shi, *Carbon* **2009**, *47*, 3538; d) H. Chen, M. B. Müller, K. J. Gilmore, G. G. Wallace, D. Li, *Adv. Mater.* **2008**, *20*, 3557; e) X. Yang, J. Zhu, L. Qiu, D. Li, *Adv. Mater.* **2011**, *23*, 2833; f) X. Yang, L. Qiu, C. Cheng, Y. Wu, Z.-F. Ma, D. Li, *Angew. Chem.* **2011**, *123*, 7463; *Angew. Chem. Int. Ed.* **2011**, *50*, 7325.

[6] H. B. Yao, H. Y. Fang, Z. H. Tan, L.-H. Wu, S.-H. Yu, *Angew. Chem.* **2010**, *122*, 2186; *Angew. Chem. Int. Ed.* **2010**, *49*, 2140.

[7] a) Z. Tang, N. A. Kotov, S. Magonov, B. Ozturk, *Nat. Mater.* **2003**, *2*, 413; b) P. Podsiadlo, A. K. Kaushik, E. M. Arruda, A. M. Waas, B. S. Shim, J. D. Xu, H. Nandivada, B. G. Pumplin, J. Lahann, A. Ramamoorthy, N. A. Kotov, *Science* **2007**, *318*, 80; c) H. B. Yao, Z. H. Tan, H. Y. Fang, S.-H. Yu, *Angew. Chem.* **2010**, *122*, 10325; *Angew. Chem. Int. Ed.* **2010**, *49*, 10127; d) J. Wang, L. Lin, Q. Cheng, L. Jiang, *Angew. Chem.* **2012**, *124*, 4754; *Angew. Chem. Int. Ed.* **2012**, *51*, 4676.

[8] Q. Cheng, M. Li, L. Jiang, Z. Tang, *Adv. Mater.* **2012**, *24*, 1838.

[9] a) A. Walther, I. Bjurhager, J. M. Malho, J. Ruokolainen, L. Berglund, O. Ikkala, *Angew. Chem.* **2010**, *122*, 6593; *Angew. Chem. Int. Ed.* **2010**, *49*, 6448; b) A. Walther, I. Bjurhager, J. M. Malho, J. Pere, J. Ruokolainen, L. A. Berglund, O. Ikkala, *Nano Lett.* **2010**, *10*, 2742.

[10] a) E. Munch, M. E. Launey, D. H. Alsem, E. Saiz, A. P. Tomsia, R. O. Ritchie, *Science* **2008**, *322*, 1516; b) A. R. Studart, L. J. Bonderer, L. J. Gauckler, *Science* **2008**, *319*, 1069.

[11] a) K. S. Novoselov, A. K. Geim, S. V. Morozov, D. Jiang, Y. Zhang, S. V. Dubonos, I. V. Grigorieva, A. A. Firsov, *Science* **2004**, *306*, 666; b) D. Li, R. B. Kaner, *Science* **2008**, *320*, 1170; c) X. Huang, Z. Yin, S. Wu, X. Qi, Q. He, Q. Zhang, Q. Yan, F. Boey, H. Zhang, *Small* **2011**, *7*, 1876.

[12] Q. He, S. Wu, Z. Yin, H. Zhang, *Chem. Sci.* **2012**, *3*, 1764.

[13] a) S. Stankovich, D. A. Dikin, G. H. B. Dommett, K. M. Kohlhaas, E. J. Zimney, E. A. Stach, R. D. Piner, S. T. Nguyen, R. S. Ruoff, *Nature* **2006**, *442*, 282; b) K. Sheng, Y. Sun, C. Li, W. Yuan, G. Shi, *Sci. Rep.* **2012**, *2*, 247.

[14] a) Z. Xu, C. Gao, *Nat. Commun.* **2011**, *2*, 571; b) H.-P. Cong, X.-C. Ren, P. Wang, S.-H. Yu, *Sci. Rep.* **2012**, *2*, 613; c) Z. Xu, H. Sun, X. Zhao, C. Gao, *Adv. Mater.* **2013**, *25*, 188; d) Z. Dong, C. Jiang, H. Cheng, Y. Zhao, G. Shi, L. Jiang, L. Qu, *Adv. Mater.* **2012**, *24*, 1856.

[15] a) X. Huang, Z. Zeng, Z. Fan, J. Liu, H. Zhang, *Adv. Mater.* **2012**, *24*, 5979; b) X. Huang, X. Qi, F. Boey, H. Zhang, *Chem. Soc. Rev.* **2012**, *41*, 666.

[16] S. Park, K. S. Lee, G. Bozoklu, W. Cai, S. T. Nguyen, R. S. Ruoff, *ACS Nano* **2008**, *2*, 572.

[17] S. Park, D. A. Dikin, S. T. Nguyen, R. S. Ruoff, *J. Phys. Chem. C* **2009**, *113*, 15801.

[18] N. V. Medhekar, A. Ramasubramaniam, R. S. Ruoff, V. B. Shenoy, *ACS Nano* **2010**, *4*, 2300.
[19] Z. An, O. C. Compton, K. W. Putz, L. C. Brinson, S. T. Nguyen, *Adv. Mater.* **2011**, *23*, 3842.
[20] Y. Gao, L.-Q. Liu, S.-Z. Zu, K. Peng, D. Zhou, B.-H. Han, Z. Zhang, *ACS Nano* **2011**, *5*, 2134.
[21] a) Y. Xu, H. Bai, G. Lu, C. Li, G. Shi, *J. Am. Chem. Soc.* **2008**, *130*, 5856; b) X. Qi, K.-Y. Pu, H. Li, X. Zhou, S. Wu, Q.-L. Fan, B. Liu, F. Boey, W. Huang, H. Zhang, *Angew. Chem.* **2010**, *122*, 9616; *Angew. Chem. Int. Ed.* **2010**, *49*, 9426; c) X. Qi, K.-Y. Pu, X. Zhou, H. Li, B. Liu, F. Boey, W. Huang, H. Zhang, *Small* **2010**, *6*, 663.
[22] O. C. Compton, S. W. Cranford, K. W. Putz, Z. An, L. C. Brinson, M. J. Buehler, S. T. Nguyen, *ACS Nano* **2012**, *6*, 2008.
[23] I.-W. P. Chen, R. Liang, H. Zhao, B. Wang, C. Zhang, *Nanotechnology* **2011**, *22*, 485708.
[24] V. Singh, D. Joung, L. Zhai, S. Das, S. I. Khondaker, S. Seal, *Prog. Mater. Sci.* **2011**, *56*, 1178.
[25] J. Liang, L. Huang, N. Li, Y. Huang, Y. Wu, S. Fang, J. Oh, M. Kozlov, Y. Ma, F. Li, R. Baughman, Y. Chen, *ACS Nano* **2012**, *6*, 4508.
[26] H. Fan, L. Wang, K. Zhao, N. Li, Z. Shi, Z. Ge, Z. Jin, *Biomacromolecules* **2010**, *11*, 2345.
[27] Q. L. Feng, F. Z. Cui, G. Pu, R. Z. Wang, H. D. Li, *Mater. Sci. Eng. C* **2000**, *11*, 19.
[28] R. Z. Wang, Z. Suo, A. G. Evans, N. Yao, I. A. Aksay, *J. Mater. Res.* **2001**, *16*, 2485.
[29] T. E. Schäffer, C. Ionescu-Zanetti, R. Proksch, M. Fritz, D. A. Walters, N. Almqvist, C. M. Zaremba, A. M. Belcher, B. L. Smith, G. D. Stucky, D. E. Morse, P. K. Hansma, *Chem. Mater.* **1997**, *9*, 1731.
[30] D. A. Dikin, S. Stankovich, E. J. Zimney, R. D. Piner, G. H. B. Dommett, G. Evmenenko, S. T. Nguyen, R. S. Ruoff, *Nature* **2007**, *448*, 457.
[31] C. Lee, X. Wei, J. W. Kysar, J. Hone, *Science* **2008**, *321*, 385.
[32] S. Pei, H.-M. Cheng, *Carbon* **2012**, *50*, 3210.
[33] S. Pei, J. Zhao, J. Du, W. Ren, H.-M. Cheng, *Carbon* **2010**, *48*, 4466.
[34] W. J. Landis, J. J. Librizzi, M. G. Dunn, F. H. Silver, *J. Bone. Miner. Res.* **1995**, *10*, 859.
[35] H. Sano, B. Ciucchi, W. G. Matthews, D. H. Pashley, *J. Dent. Res.* **1994**, *73*, 1205.
[36] A. Satti, P. Larpent, Y. Gun'ko, *Carbon* **2010**, *48*, 3376.
[37] K. W. Putz, O. C. Compton, M. J. Palmeri, S. T. Nguyen, L. C. Brinson, *Adv. Funct. Mater.* **2010**, *20*, 3322.
[38] H. Lu, Z. Chen, C. Ma, *J. Mater. Chem.* **2012**, *22*, 16182.
[39] H. A. Becerril, J. Mao, Z. Liu, R. M. Stoltenberg, Z. Bao, Y. Chen, *ACS Nano* **2008**, *2*, 463.
[40] D. Li, M. B. Muller, S. Gilje, R. B. Kaner, G. G. Wallace, *Nat. Nanotechnol.* **2008**, *3*, 101.

